Since January 2020 Elsevier has created a COVID-19 resource centre with free information in English and Mandarin on the novel coronavirus COVID-19. The COVID-19 resource centre is hosted on Elsevier Connect, the company's public news and information website.

POTENTIAL CLINICAL RELEVANCE

Nanomedicine: Nanotechnology, Biology, and Medicine
10 (2014) 819–829

Original Article

nanomedjournal.com

Magnetic nanoparticle-based immunoassay for rapid detection of influenza infections by using an integrated microfluidic system

Lien-Yu Hung, PhD[a], Jui-Cheng Chang, PhD[b], Yi-Che Tsai[c], Chih-Chia Huang, PhD[b], Chih-Peng Chang, PhD[c], Chen-Sheng Yeh, PhD[b,**], Gwo-Bin Lee, PhD[a,d,e,*]

[a]*Department of Power Mechanical Engineering, National Tsing Hua University, Hsinchu, Taiwan*
[b]*Department of Chemistry, National Cheng Kung University, Tainan, Taiwan*
[c]*Department of Microbiology and Immunology, National Cheng Kung University, Tainan, Taiwan*
[d]*Institute of Biomedical Engineering, National Tsing Hua University, Hsinchu, Taiwan*
[e]*Institute of NanoEngineering and Microsystems, National Tsing Hua University, Hsinchu, Taiwan*

Received 4 April 2013; accepted 19 November 2013

Abstract

Magnetic manganese ferrite ($MnFe_2O_4$) nanoparticles with approximately 100 nm in diameter were used to improve the performance of an immunoassay for detecting influenza infections. The synthesized nanoparticles were tested for long-term storage to confirm the stability of their thermal decomposition process. Then, an integrated microfluidic system was developed to perform the diagnosis process automatically, including virus purification and detection. To apply these nanoparticles for influenza diagnosis, a micromixer was optimized to reduce the dead volume within the microfluidic chip. Furthermore, the mixing index of the micromixer could achieve as high as 97% in 2 seconds. The optical signals showed that this nanoparticle-based immunoassay with dynamic mixing could successfully achieve a detection limit of influenza as low as 0.007 HAU. When compared with the 4.5-μm magnetic beads, the optical signals of the $MnFe_2O_4$ nanoparticles were twice as sensitive. Furthermore, five clinical specimens were tested to verify the usability of the developed system.

From the Clinical Editor: In this study, magnetic manganese ferrite nanoparticles were used to improve the performance of a novel immunoassay for the rapid and efficient detection of influenza infections.

Key words: Influenza; Microfluidics; Nanoparticles; Surface modification

Viral infectious diseases have been a serious threat to human health worldwide. The notorious acquired immunodeficiency syndrome instigated by the human immunodeficiency virus (HIV), for example, has caused the death of more than 10 million people for more than three decades.[1] Another serious disease is the severe acute respiratory syndrome (SARS), caused by SARS coronavirus, which broke out in 2002.[2] More recently, in the winter of 2012, both norovirus and influenza virus caused

Abbreviations: α-A-NP, anti-influenza A nucleoprotein; BSA, bovine serum albumin; C^+, normalized concentration; CCD, charge-coupled device; D^+, normalized location across the micromixer; DI, deionized; DMEM, Dulbecco's modified Eagle's medium; ELISA, enzyme-linked immunosorbent assay; EMVs, electromagnetic valves; FIA, fluorescence immunoassay; HAU, hemagglutin units; JCPDS, Joint Committee on Powder Diffraction Standards; LOC, lab-on-a-chip; LBL, layer-by-layer; mAbs, monoclonal antibodies; MDCK, Mardin–Darby canine kidney cells; MEMS, Micro-electro-mechanical systems; EDC, *N*-(3-dimethylaminopropyl)-*N*-ethyl carbodiimide hydrochloride; One-way ANOVA, one-way analysis of variance; P123, poly(ethylene oxide)–poly (propylene oxide)–poly(ethylene oxide) triblock copolymer; PAA, poly(acrylic acid); PAH, polyallylamine hydrochloride; PBS, phosphate-buffered saline; PCR, polymerase chain reaction; PDMS, poly(dimethylsiloxane); PE, R-phycoerythrin; PEI, poly(ethyleneimine)); PMT, photo-multiplier tube; RB, round bottom; SARS, severe acute respiratory syndrome; TEM, transmission electron microscope; TPCK, type XIII l-1-tosylamide-2-phenylethyl chloromethyl ketone; UV, ultraviolet; XRD, X-ray diffractometer.

The preliminary results from this paper were presented at the 2012 IEEE International Conference on Nano/Molecular Medicine and Engineering (IEEE-NANOMED 2012), Bangkok, Thailand, 2012.

*Correspondence to: Gwo-Bin Lee, Department of Power Mechanical Engineering, Institute of Biomedical Engineering and Institute of NanoEngineering and Microsystems, National Tsing Hua University, Hsinchu, Taiwan.

**Correspondence to: Chen-Sheng Yeh, Department of Chemistry, National Cheng Kung University, Tainan, Taiwan.

E-mail addresses: csyeh@mail.ncku.edu.tw (C.-S. Yeh), gwobin@pme.nthu.edu.tw (G.-B. Lee).

1549-9634/$ – see front matter © 2014 Elsevier Inc. All rights reserved.
http://dx.doi.org/10.1016/j.nano.2013.11.009

widespread illness and infected millions of people. People infected with norovirus can develop acute gastroenteritis and become ill with influenza, causing sudden fever and whole-body achiness, as well as lung and heart diseases.[3] Furthermore, the influenza virus, which causes the flu, caused several historic pandemics; for instance, the Spanish Flu of 1918 claimed 27 million lives worldwide. The Hong Kong Flu in 1968 and the Bird Flu in 2004 also caused numerous deaths worldwide. The Swine Flu outbreak in June 2009 in Mexico caused serious concern because of the hydride genome of that virus.[4,5] Therefore, the capability to detect influenza infections rapidly and provide immediate and appropriate clinical treatment is an important need that needs to be addressed.

To diagnose influenza infection accurately, various types of diagnostic methods, such as viral culture, enzyme-linked immunosorbent assay (ELISA),[6] fluorescence immunoassay (FIA),[7] and molecular diagnosis using a real-time polymerase chain reaction (PCR),[8] have already been developed and applied in hospitals and laboratories. However, they are labor-intensive processes performed by well-trained personnel, and also require a substantial amount of bench-top equipment. Recently, with the development of micro-electro-mechanical systems (MEMS) technologies, an increasing number of miniature biomedical systems have demonstrated the potential for virus detection. For instance, a nano-cantilever beam operating as a mass detector was developed for the detection of viral particle[9]; this type of microsystem was further used for virus-specific antibodies to selectively detect pathogens.[10,11] However, sample pre-treatment and virus purification are still challenging to achieve in the cantilever beam sensing system.

In recent years, magnetic bead-based immunoassays have been integrated with microfluidic systems to realize effective micro-total-analysis system or lab-on-a-chip systems for pathogen detection.[12,13] Magnetic bead-based immunoassays were modified based on the sandwich-like immunoassays. Specific antibodies were coated on beads, which enabled the specific isolation and collection of target cells or viruses by using a magnetic force.[14] For instance, microfluidic systems demonstrating the capability of executing separations and detection of DNA fragments with small amounts of reagents in a single microfluidic device were achieved.[15,16] Rapid viral detection has also been demonstrated by several research groups.[17,18] For example, a microfluidic device with bead-based viral purification and on-chip reverse transcriptase PCR capabilities was applied to specifically detect dengue virus and enterovirus 71.[17] An integrated micro-flow cytometry using the bead-based immunoassay approach has demonstrated automatic detection of the dengue virus down to a concentration of 10^3 PFU/mL in 40 min.[18] Yet another integrated microfluidic system has achieved rapid detection in as little as 15 min which has been realized while using clinical specimens.[19,20] However, the magnetic beads used in previous studies are approximately 4.5 μm in diameter, which is much bigger than the influenza virus (approximately 100 nm in diameter). The incomparable size between beads and viruses can affect the detection signal and cause relatively high background noise. Using beads with smaller sizes and larger surface area may be beneficial for target detection.

With the advancement of nanotechnology, numerous nanomaterials have been developed for their unique properties. For instance, fullerenes and carbon nanotubes show high heat conductivity, electrical conductivity, and relative low chemical activity. They have even been used for medical studies associated with bacteria, viruses, and cancer cells.[21–23] Nanoparticles have also been developed for detecting avian flu in red blood cells[24] or alpha-fetoprotein in serum[25] because of their uniform distribution, long-term stability and bio-compatibility. Among them, magnetic nanoparticles have been applied in molecular imaging because of their outstanding magnetic-spin structures such that they could enhance magnetic resonance imaging.[26–28] Moreover, magnetic nanoparticles have advantages including multiplexing, reduced analysis time and selectivity control. Furthermore, with the development of microfluidic systems, magnetic nanoparticles have been used for immunoassay applications that involved a simple microfluidic chip. However, only immunoglobulin G was used as a test model and no disease detection was demonstrated.[29] For instance, superparamagnetic nanoparticles have been used to capture pathogenic microorganisms or nanometer-size particles, such as virions.[30,31] Immunoglobulin E detection in diagnosing allergies is another application of magnetic nanoparticles.[32] The high capture rate, throughput, and sample pre-concentration, as compared with the traditional assay, have been demonstrated.[33]

In this study, it is the first attempt to apply nanoparticles, by using an integrated microfluidic system that involves characterized micro-devices working with magnetic $MnFe_2O_4$ nanoparticles for influenza detection with a FIA. By using this approach, the detection limit of the diagnosis is expected to improve because of the large surface-to-volume ratio of nanoparticles. These well-produced stable magnetic $MnFe_2O_4$ nanoparticles are further combined with a layer-by-layer (LBL) surface modification process to reduce the background noise due to non-specific adhesion of nanoparticles. An integrated microfluidics system for detection of influenza infectious in 20 min has been demonstrated and may be promising for rapid diagnosis in the near future.

Methods

Working principle of the diagnosis assay

Figure 1 shows a simplified diagram illustrating the diagnosis assay used in this study. The magnetic nanoparticles were surface-coated with anti-influenza A nucleoprotein (α-A-NP) monoclonal antibodies (mAbs), pre-loaded in a micromixer, and incubated with purified viral particle samples for 5 min (Figure 1, *A*). The purification of nanoparticle–virus complexes was realized by washing out non-specific interferences when an external magnetic field was applied for 2 min (Figure 1, *B*). After washing, the direct-conjugated R-phycoerythrin (PE) developing mAbs (α-A-NP–PE mAbs) was transported into the micromixer to incubate with the nanoparticle–virus complexes for 5 min (Figure 1, *C*). The non-binding interferences were washed away and the purification of the nanoparticle–virus-developing mAb complexes with the similar process. Finally, an optical detection module was used to detect the optical signal of the purified nanoparticle–virus-developing

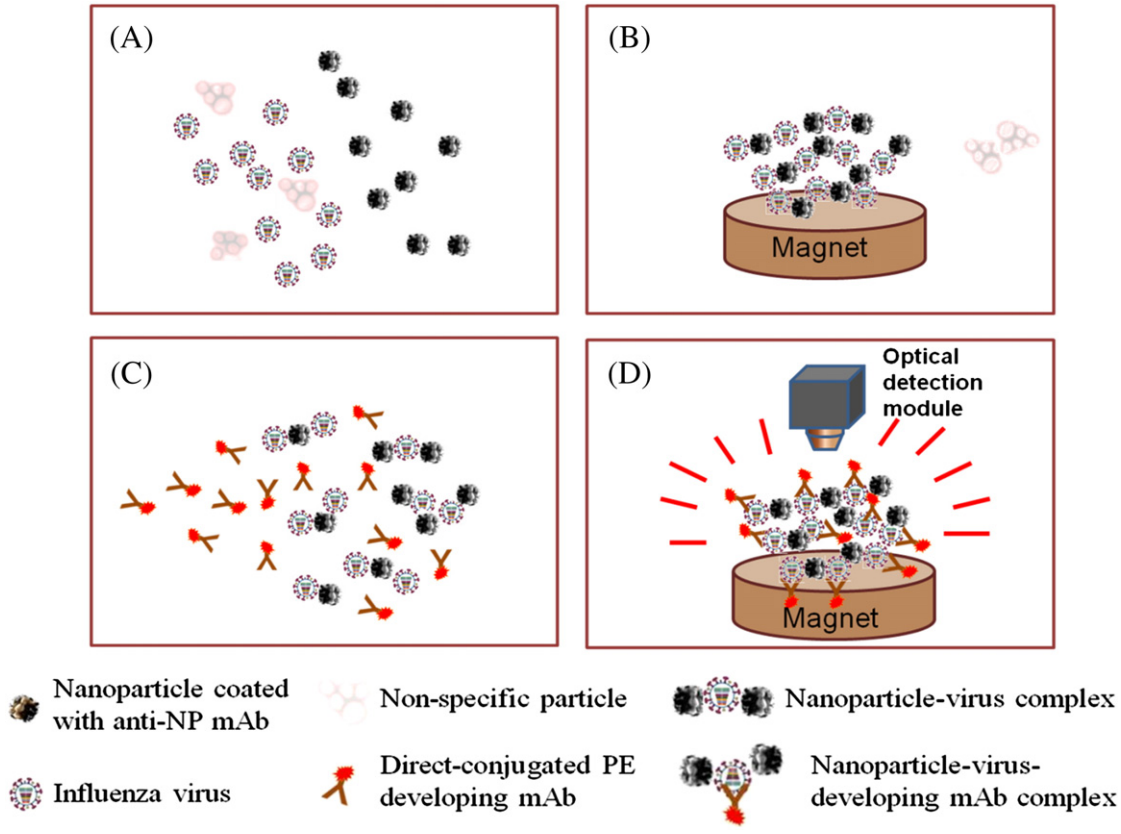

Figure 1. A schematic diagram of the magnetic $MnFe_2O_4$ nanoparticle bead-based immunoassay process used in this study. **(A)** Mix viral particles and surface-modified mAbs magnetic nanoparticles for 5 min. **(B)** Collect the nanoparticle–virus complexes and wash out the non-specific materials. **(C)** Transport the α-A-NP–PE mAbs into the mixing chamber and mix them with the nanoparticle–virus complexes for 5 min. **(D)** Collect the nanoparticle–virus-mAb-PE complexes, wash and detect the signals by using the optical detection module.

mAbs complexes (Figure 1, *D*). All detailed information about the on-chip experimental procedures regarding the magnetic nanoparticle bead-based microfluidic immunoassay is listed in Supplemental Table 1.

Fabrication of microfluidic chip and surface modification

The microfluidic chip in the current study was composed of three layers: one thick poly(dimethylsiloxane) (PDMS) air-channel layer, one thin PDMS liquid-channel layer, and one glass substrate spin-coated with PDMS (Figure 2, *A*). A schematic illustration of the developed microfluidic chip composed of washing buffer chambers, α-A-NP–PE mAbs chambers, micropumps, normally closed microvalves, and micromixers for performing the entire diagnosis process is shown in Figure 2, *B*, which consisted of eight reaction units and could test eight samples in one chip. Figure 2, *C* shows a photograph of the chip with dimensions measured to be 73 mm × 55 mm. Note that the light red color indicates the air channels and the light blue color indicates the liquid channels in this figure.

The shape and size of the detection and incubation chambers were especially designed for controlling the magnetic nanoparticles. The original incubation chambers contained microfluidic side channels, where nanoparticles might adsorb along the edges with the dead-volume regions.[19,20] Therefore, the micromixer was modified into a circular shape to reduce the adsorption of the magnetic nanoparticles.[34] However, the previous circular-micromixer had a large mixing area, which limited the magnetic nanoparticles collection. In this study, the circular diameter of the micromixer was reduced from 15,000 μm to 2,600 μm, indicating that the working PDMS membrane area was also reduced. Consequently, both positive and negative forces were provided for efficient mixing. Therefore, a negative gauge pressure of −80 kPa and a positive gauge pressure of 10 psi were used in this study.

In addition to the microfluidic structures, this study applied poly(ethyleneimine) (PEI) and poly(acrylic acid) (PAA) with subsequent cross-linking for long-term surface modification on the PDMS channel surface such that it may remain hydrophilic.[35] As shown schematically in Figure 2, *D*, a surface modification process was performed to form functional groups on the PDMS surface. Firstly, poly(ethylene oxide)–poly (propylene oxide)–poly(ethylene oxide) triblock copolymer (Pluronic P123, MW 5750, 2.5% [wt/vol]) in 99% aqueous ethanol, was used to cover the PDMS surface for 15 min. Secondly, the PDMS surface with a thin layer of the Pluronic P123 was layered with PAA (MW 100,000, 1% [wt/vol], in

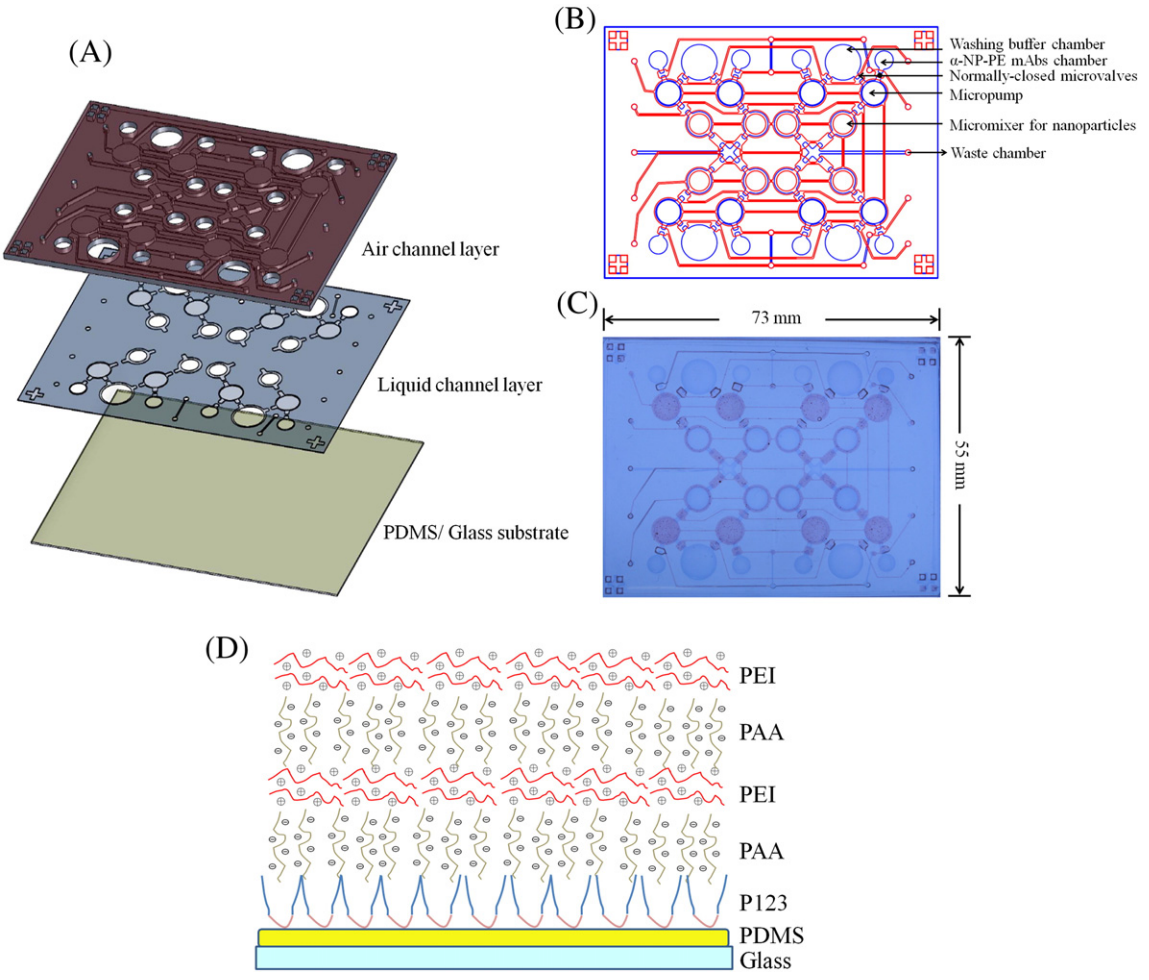

Figure 2. **(A)** An exploded view of the microfluidic chip consisting of two PDMS layers and one glass/PDMS substrate. **(B)** A schematic illustration of the microfluidic chip. **(C)** A photograph of the microfluidic chip. **(D)** A schematic illustration of PDMS surface modification with P123, PAA, and PEI multilayers.

deionized [DI] water) for 15 min. Thirdly, the PDMS surface was coated with a PEI solution (MW 75,000, 0.25% [wt/vol], in DI water) for 15 min. This sequence of surface modification was repeated twice to obtain the desired thickness of polyelectrolyte multilayers and the native hydrophobic PDMS surface could be surface-modified to hydrophilic.[36]

Synthesis and characterization of nanoparticles

In order to target influenza viruses that infected on mock cells, the targeted materials (the surface of $MnFe_2O_4$ nanoparticles will be conjugated with influenza A anti-body) must be hydrophilic. Based on the process reported in the literature,[37] the method of MnFeO nanoparticles synthesis is in hydrophobic phase. Therefore, the hydrophobic MnFeO nanoparticles must be transferred to the hydrophilic phase and then conjugated with influenza A anti-body. In a typical synthesis procedure, iron (III) acetylacetonate [$Fe(acac)_3$, 1.4 g, Aldrich], manganese (II) acetate [$Mn(ac)_2$, 0.346 g, Alfa Aesar], oleic acid (90%, 3.36 mL, Aldrich) and trioctylamine (98%, 15 mL, Aldrich) were first mixed in a two-neck round bottom (RB) flasks (precursor 1) and heated up to 305 °C at a heating rate of 33 °C/min and maintained at this temperature for 30 min, and then reduced to 270 °C. The average particle size of nanoparticles obtained in this treatment was 40 nm (Figure 3, *A*). Another solution (precursor 2) with a total volume of 12 mL was prepared in a separate RB by mixing $Fe(acac)_3$ (0.84 g), $Mn(ac)_2$ (0.208 g), oleic acid (90%, 6.12 mL) and trioctylamine (98%, 5 mL) and heated up to 150 °C, and then maintained at this temperature for 20 min. The precursor 2 was then added into the precursor 1 and heated up to 305 °C for 30 min, and then reduced to 270 °C. The process of adding the precursor 2 and temperature programming was repeated four times and particle size obtained in each step was 57, 63, 75 and 95 nm, respectively (Figure 3, *A*). The final products were separated by 8000-rpm centrifugation for 10 min, washed three times with ethanol and dispersed in toluene.[37,38] A series of transmission electron microscope (TEM) images of the magnetic $MnFe_2O_4$ nanoparticles are shown in Figure 3. The size of the synthesized nanoparticles can be fine-tuned to an average size of 98 ± 19.5 nm with this approach.

To confirm the stability of these nanoparticles, these products were tested under TEM and UV–Vis spectrum analysis. The

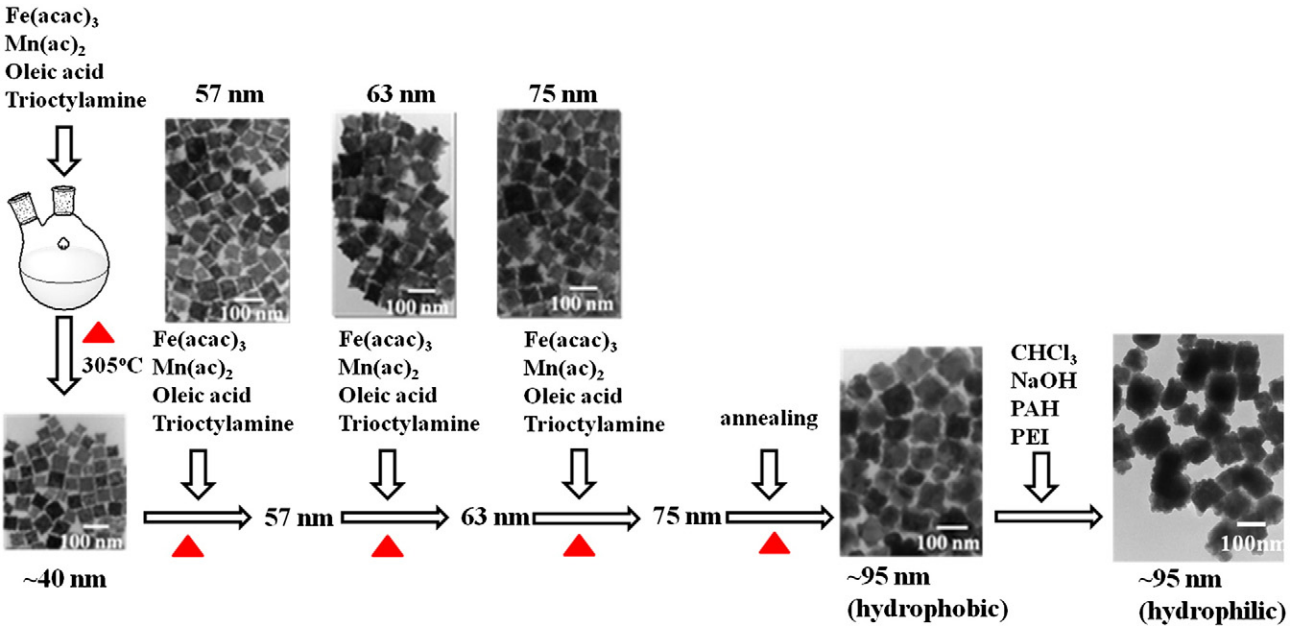

Figure 3. A schematic diagram of the $MnFe_2O_4$ nanoparticle production process used in this study. $Fe(acac)_3$, $Mn(ac)_2$, oleic acid, and trioctylamine were first mixed and heated to 305 °C. After $Fe(acac)_3$, $Mn(ac)_2$, oleic acid, and trioctylamine were added four times into the synthesis solution in different concentrations, the size of nanoparticles grew to approximately 100 nm. Subsequently, the nanoparticles were transformed from hydrophobic to hydrophilic with $CHCl_3$, NaOH, PAH and PEI reaction.

crystalline structures were further identified using an X-ray diffractometer (XRD) analysis with nanoparticles preserved for three months. TEM analysis was performed using JEOL 2100 F at 200 kV and PHILIPS CM-200 at 200 kV (Hitachi H-7500, Japan). UV–Vis optical absorption spectra were recorded on a spectrophotometer (Hewlett-Packard Company, Palo Alto, CA, USA). The XRD spectrum used Cu Kα radiation (λ = 1.54056 Å) at 30 kV and 30 mA (Shimadzu XRD-7000S X-Ray Diffractometer, Japan).

Preparation of reagents, virus and cell lines

This microfluidic system demonstrated its specificity in capturing the influenza virus by using the specific mouse α-A-NP mAbs (H16L-10-4R5 cell line [HB-65], ATCC, USA). They were conjugated onto the surface of $MnFe_2O_4$ nanoparticles to form α-A-NP mAb-conjugated nanoparticles. The process for these custom-developed mAbs and α-A-NP–PE mAbs was used to conjugate the PE fluorescent dye directly by using a commercial kit, the EasyLink R-Phycoerythrin Conjugation Kit (Abcam, UK). Note that magnetic beads (M450, Dynabeads® M-450 Epoxy, Invitrogen, USA stock concentration = 4×10^8 beads/mL, 4.5-μm diameter) were also used in this study for comparing the performance of developed $MnFe_2O_4$ nanoparticle assays. Detailed information on this measurement process conjugating $MnFe_2O_4$ nanoparticles and M450 beads with α-A-NP mAbs and α-A-NP–PE mAbs is shown in Supplemental Information (SI) section II and could be also found in a previous study.[20]

Influenza A/H1 (subtype of H1N1, 97N510H1) was used to verify the performance of the integrated microfluidic system with magnetic nanoparticles. All of the tested influenza viruses were infected in Mardin–Darby canine kidney (MDCK) cells.[39] Detailed information about viral culture, purification and tittering methods could be found in the SI section III. Clinical specimens were obtained from the Microbiology and Immunology Laboratory of National Cheng Kung University (NCKU) and the Department of Pathology of NCKU Hospital in Taiwan. A total of five clinical samples were collected. Two of them were known negative samples and the other three samples were positive samples. All viral samples were stored at −80 °C until tested. The influenza viruses were diluted in serial dilutions four times to determine the limit of detection (LOD). They were diluted with a 4 °C 1× PBS buffer to form various viral concentrations ranging from 1:128 with a 4^{-2} dilution (8 HAU/50 μL) to 1:128 with a 4^{-7} dilution (0.007 HAU/50 μL). The 1× PBS buffer was used as negative control (NC) for background noise testing.

Experimental setup and statistical analysis

A custom-made, programmable control system, electromagnetic valves (EMVs, SD70M-6BG-32, SMC, Japan), a digital controller (8051 microcontroller, model AT89C51 24PC, ATMEL, USA), a vacuum pump (UN-90 V, UNI-CROWN Inc., Taiwan), and an air compressor (Gast Manufacturing Inc., USA) were used for the automatic process of the microfluidic system. These experimental setups were used to drive all of the microfluidic components, including micropumps and micromixers. The driving frequencies of the EMVs were regulated for the mixing index testing. The red ink was pre-loaded in the micromixer to calibrate the mixing index. Detailed information on this measurement process, the mixing index measurement and calculation results can be found in the SI section V and also in previous work.[19]

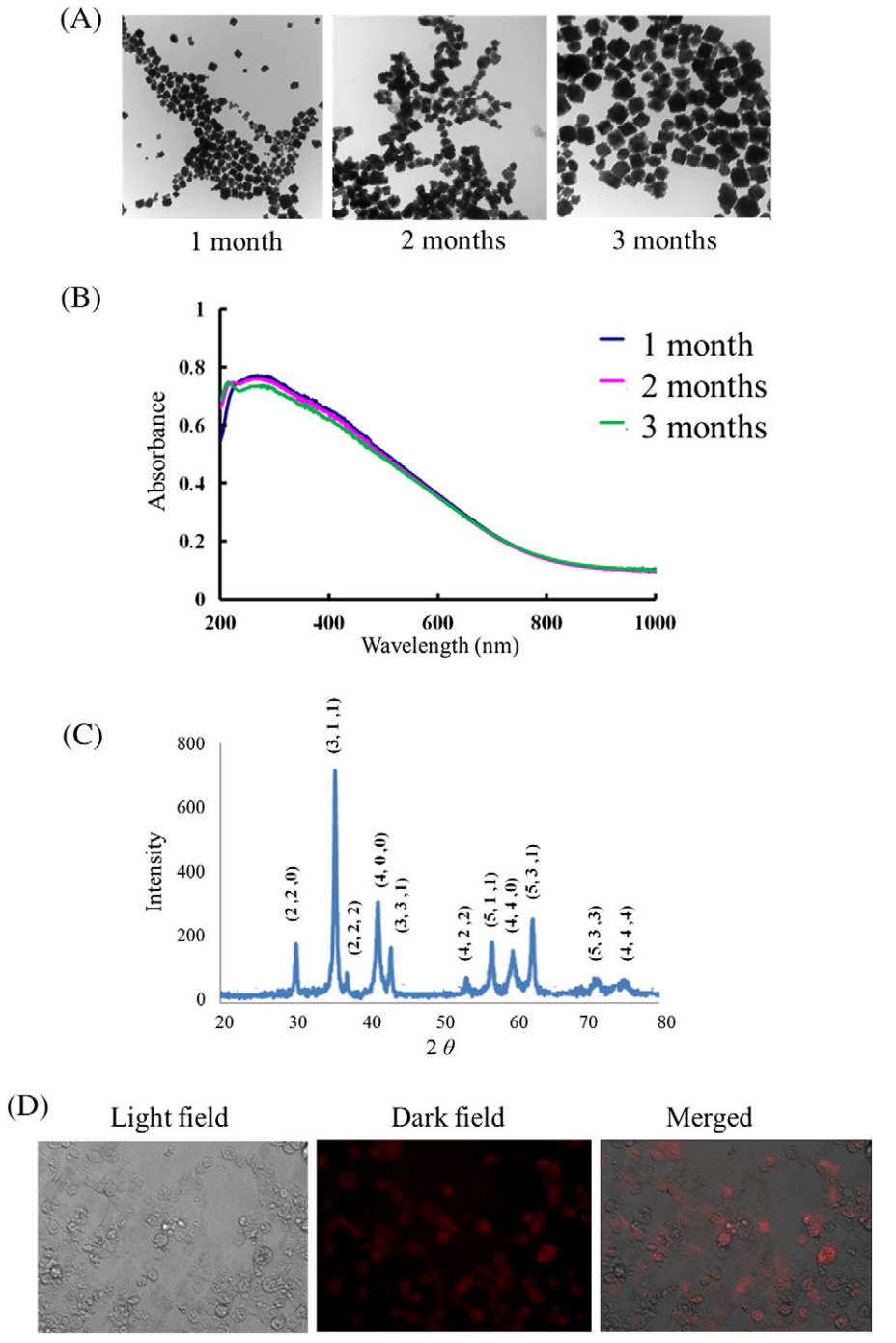

Figure 4. **(A)** A series of TEM images for magnetic $MnFe_2O_4$ nanoparticles from 1 to 3 months. **(B)** Optical absorption spectra of the nanoparticles for three months. **(C)** X-ray diffraction (XRD) spectrum of nanoparticles samples. **(D)** A series of microscopic images for testing the specific mAbs activity using the MDCK cell line. The cells were infected by influenza virus and PE fluorescent signals were detected in the dark field.

In the optical detection process, a fluorescence microscope, combined with a photo-multiplier tube (PMT, R928, Hamamatsu, Japan), a mercury lamp (MODEL C-SHG1, Nikon, Japan), several optical components containing a collimation lens, an objective lens (Nikon LU Plan 10×/0.30 A, Nikon, Japan), and three fluorescence filters (Nikon G-2A, Nikon, Japan) were used. The mercury lamp was used to excite the PE dye, and the excited fluorescent signals were first emitted through an excitation filter (535/25-nm band-pass [BP], Nikon, Japan). Subsequently, the emitted signals from the PE dye were passed through a dichroic mirror (565-nm cut-off wavelength, Nikon, Japan) and other signals were filtered by using a barrier filter (590-nm long-pass [LP], Nikon, Japan).[19] The fluorescence decay analysis of nanoparticle in PE was shown in SI section VIII.

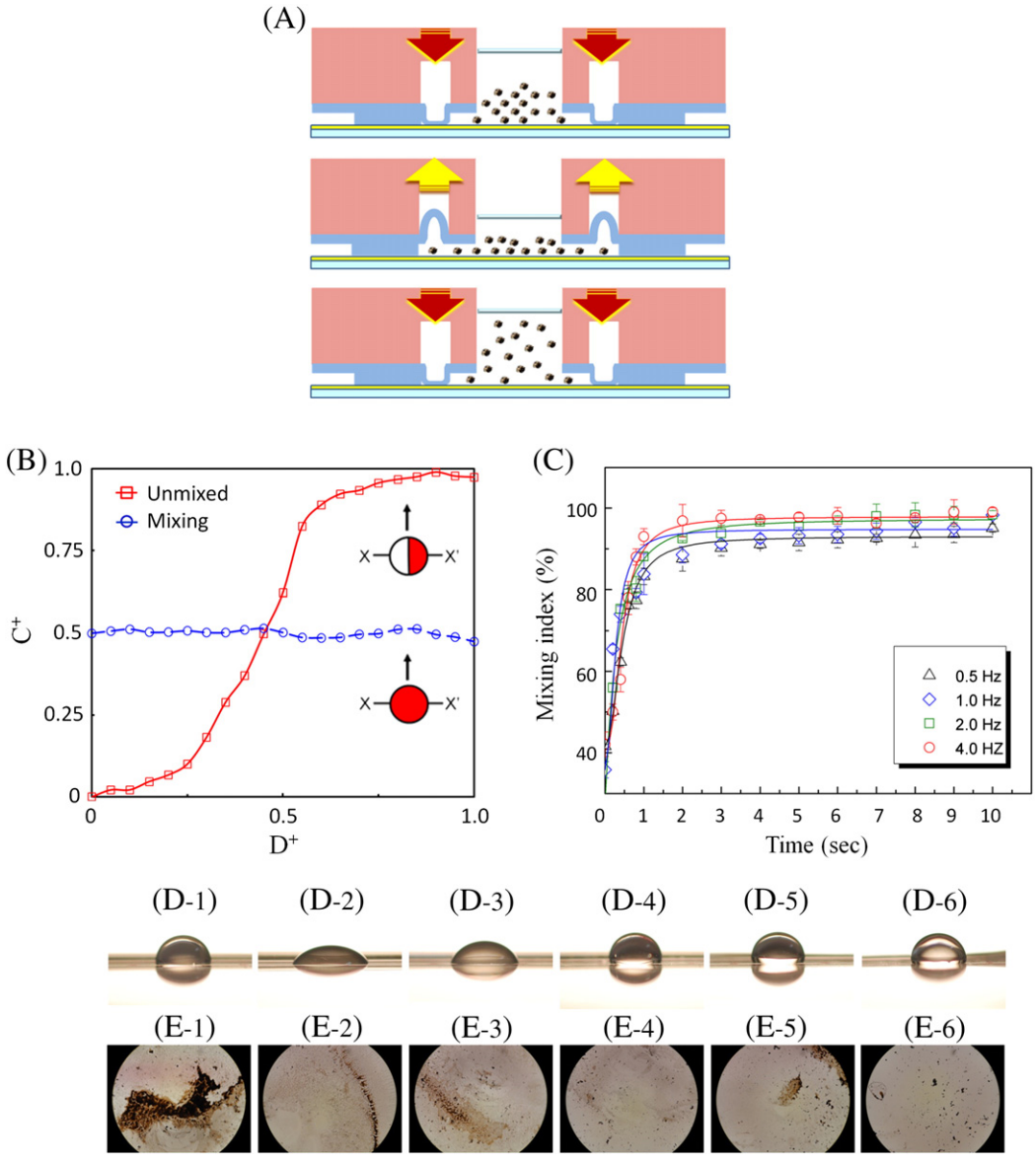

Figure 5. **(A)** A schematic illustration of the working principle for the micromixer operated with both vacuum and compressed air. **(B)** Normalized concentration profile across the micromixers. **(C)** Mixing index while operated at different driving frequencies. **(D)** Contact angle measurement for different surfaces: **(D-1)** non-modified PDMS, 98.4° ± 5.4°; **(D-2)** P123 modified surface, 48.0° ± 2.6°; **(D-3)** P123/PAA modified surface, 68.6° ± 4.6°; **(D-4)** P123/PAA/PEI modified surface, 103.3° ± 0.9°; **(D-5)** P123/PAA_2/PEI modified surface, 101.7° ± 2.7°; **(D-6)** P123/PAA_2/PEI_2 modified surface, 111.4° ± 3.2°. **(E-1–E-6)** After surface modification, the non-specific adsorption of nanoparticles in the micromixer could be observed.

One-way analysis of variance (one-way ANOVA) by using Microsoft Excel software was applied to test the optical signal difference between negative specimens (specimens 1 and 2) and positive specimens (specimens 3, 4 and 5). Detailed ANOVA analysis and calculation results can be found in the SI section IX.

Results

Nanoparticles characterization

First, the long-term stability of these magnetic $MnFe_2O_4$ nanoparticles was tested under a TEM, an UV–Vis spectrum, and an XRD spectrum analysis after a storage period of 1, 2, or 3 months. As shown in Figure 4, *A*, under the TEM analysis, these nanoparticles were measured to be approximately 100 nm in diameter and showed to no little aggregation and truncation. Furthermore, even after a 3-month preservation, these nanoparticles still maintained reasonable uniformity. Figure 4, *B* shows the UV–Vis spectrum of magnetic nanoparticles, which exhibits an absorption range from 200 to 600 nm, with a maximum absorption at 300–350 nm. Three-month preservation results also show no significant band shift. In addition, XRD analysis in Figure 4, *C* shows a consistent diffraction pattern of the magnetic nanoparticles for the 3-month analysis. The eight peaks observed at 2θ—30.54° (220), 36.00° (311), 37.64° (222), 43.76° (400), 54.33° (422), 57.91° (511), 63.62° (440), and 75.30° (533)—indicated intact crystalline structures.

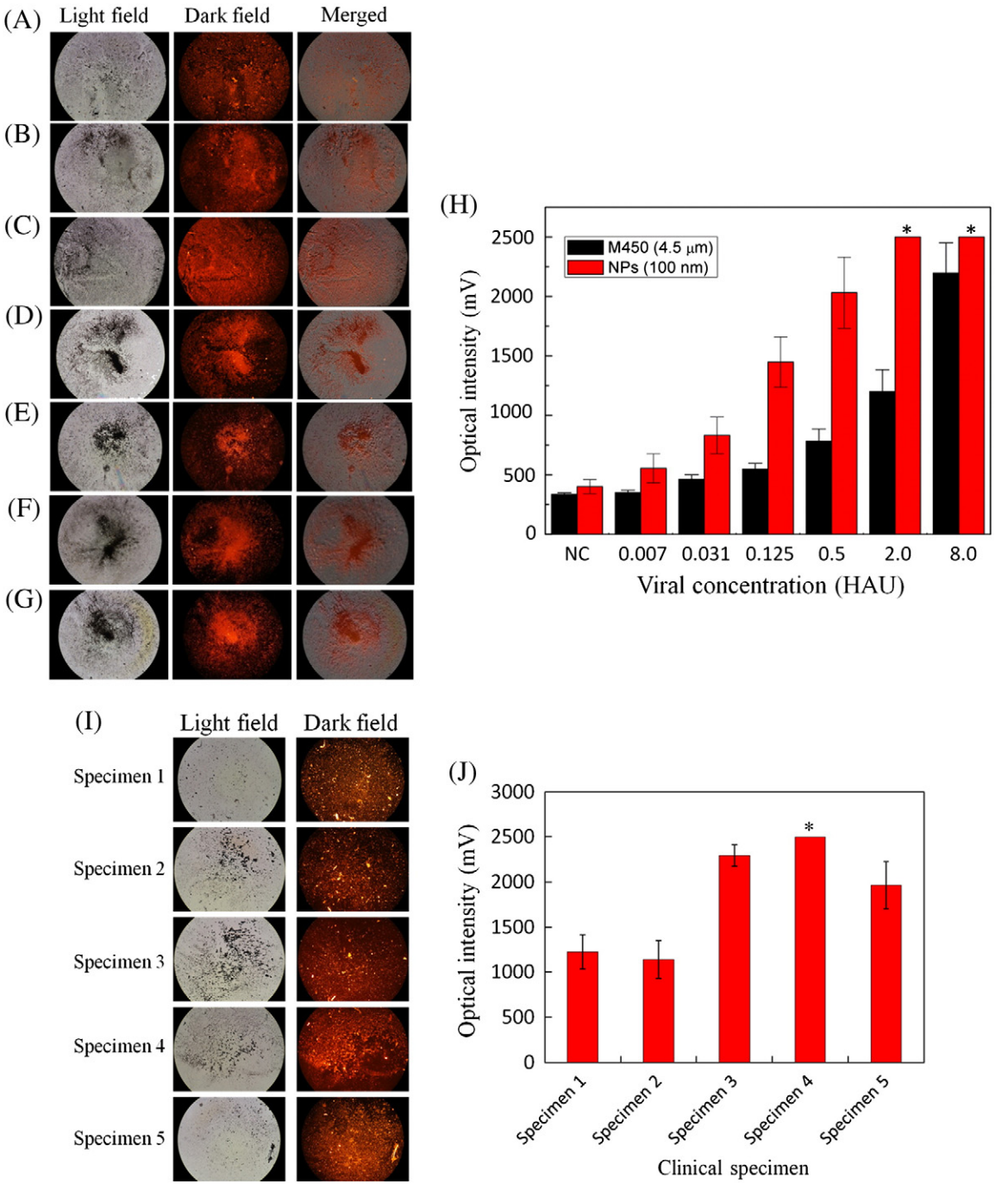

Figure 6. A series of optical images for magnetic $MnFe_2O_4$ nanoparticle complexes with different concentration of the influenza A virus. **(A)** 1 × PBS as negative control (NC), **(B)** 0.007, **(C)** 0.03, **(D)** 0.125, **(E)** 0.50, **(F)** 2.0 and **(G)** 8.0 HAU. **(H)** The comparison of optical signals between M450 beads and nanoparticles, from NC to 8.0 HAU: the measurements of nanoparticle tests were 440 ± 39, 557 ± 88, 860 ± 135, 1449 ± 183, 2032 ± 279, 2500 and 2500 mV, and the measurements of M450 were 368 ± 15, 390 ± 22, 462 ± 29, 531 ± 37, 774 ± 52, 1199 ± 155 and 2198 ± 233 mV. **(I)** A series of fluorescence images for nanoparticle complexes with clinical specimens. **(J)** Optical intensity histogram of pre-clinical tests from nanoparticles was measured to be 1225 ± 191, 1140 ± 212, 2295 ± 120, 2500 and 1964 ± 258 mV (n = 3), with one-way ANOVA analysis, $F(1,3) = 27.52 > 10.13$, $P = 0.01 < 0.05$, showing that negative and positive specimens were significantly different. *Note that the high-concentration influenza viral samples, **(H)** 2.0 and 8.0 HAU and **(J)** specimen 4 exhibit optical signals that are higher than the maximum value of the optical detection system (2500 mV).

α-A-NP mAbs binding performance

The binding activity of mAbs after conjugating onto nanoparticles was tested against influenza-infected MDCK cells. After viral infection, the viral particles remained on the cells. By further modifying the mAbs with PE fluorescent dye, the binding of mAb–nanoparticle complex to the cells can be visualized. As shown in Figure 4, *D*, since the cells were

infected by the influenza virus, nanoparticles bound with α-A-NP–PE mAbs captured the influenza-infected cells. This shows that fluorescent signals could be detected successfully. Detailed information about other control testing of the non-viral cells and infected cells with control nanoparticles is provided in Supplemental Figure 1.

Characterization of the integrated microfluidic system and surface modification

This integrated microfluidic system equipped with the modified micromixer for the dynamic mixing of nanoparticles was further tested. Figure 5, *A* shows the cross-sectional view of the micromixer. Note that both vacuum and compressed air were used to drive these micromixers. Micromixers with diameters of 2000 μm, 2300 μm, and 2600 μm were tested and the mixing index was evaluated by measuring the concentration distribution along a cross section of the mixing chamber. Note that 1 μL of red ink and 50 μL of DI water were pre-loaded into the mixing chamber to measure the mixing index of the micromixer. Figure 5, *B* shows the normalized concentration (C^+) across the normalized location (D^+) of the micromixer (X–X′ line). In the unmixed state, C^+ shows significant difference from low to high ink concentration; after mixing, C^+ value is the same for all area within the mixing chamber. The detailed information regarding the calculation of mixing index could be found in the SI section V. The optimization of the micromixer was also explored by measuring the mixing index at different driving frequencies (0.5, 1.0, 2.0, and 4.0 Hz, respectively) under an applied gauge pressure of −80 kPa and 10 psi. As shown in Figure 5, *C*, the experimental data revealed that a mixing index of as high as 97% can be realized after mixing for 2 seconds. The micromixer was then determined to be actuated at 4.0 Hz with an applied gauge pressure of both −80 kPa and 10 psi for performing the nanoparticle immunoassay. Consequently, efficient mixing within the mixing chamber can be generated for incubating the bio-samples.

In order to minimize non-specific adsorption of positively charged nanoparticles to PDMS, the PDMS surfaces in the microfluidic device were modified with P123, PAA, and PEI to form the polyelectrolyte multilayers. The formation of the multilayers was verified by the contact angle method. Comparing the contact angles between the cases before and after surface modifications (Figures 5, *D*-1 to *D*-6), the contact angle was measured according to the different layers of surface modification from 98.4° ± 5.4° in a non-modified PDMS (Figure 5, *D*-1), 48.0° ± 2.6° in a P123-modified surface (Figure 5, *D*-2), 68.6° ± 4.6° in a P123/PAA-modified surface (Figure 5, *D*-3), 103.3° ± 0.9° in a P123/PAA/PEI-modified surface (Figure 5, *D*-4), 101.7° ± 2.7° in a P123/PAA_2/PEI-modified surface (Figure 5, *D*-5) to 111.4° ± 3.2° in a P123/PAA_2/PEI_2-modified surface (Figure 5, *D*-6). Importantly, non-specific adsorption of the nanoparticles was explored for the cases before and after the surface modification. Figures 5, *E*-1 to *E*-6 clearly show that non-specific adsorption of $MnFe_2O_4$ nanoparticles was evident on the non-modified surface, but became substantially reduced on the P123/PAA_2/PEI_2-modified surface (Figure 5, *E*-6). It was therefore determined to perform the diagnostic assay in this condition.

Limit of detection

Purified influenza viral particles were then used for testing the detection limit of the developed diagnostic assay. Virus with different concentrations in serial four-time dilutions (8.0, 2.0, 0.50, 0.125, 0.031, and 0.007 HAU, respectively) were tested. Note that the entire process can be performed within 20 min. Compared with a 1× PBS buffer as a negative control (NC) (Figures 6, *A*-*G*), the optical signals for the detection of influenza virus in the microfluidic system with different viral concentrations were shown. The optical signals for samples with concentrations of 8.0, 2.0, 0.50, 0.125, 0.031, 0.007 HAU and NC were measured to be 2500, 2500, 2032 ± 279, 1449 ± 183, 860 ± 135, 557 ± 88, and 440 ± 39 mV (n = 3), respectively. Note that the maximum optical signal of the PMT was 2500 mV. Therefore, the first two cases were saturated signals. The merged images also showed that the PE fluorescence was located in the magnetic nanoparticles. Therefore, influenza virus A could be successfully detected with this approach. The limit of detection was then determined to be 0.007 HAU.

Figure 6, *H* compares the limit of detection between the M450 magnetic beads and the magnetic nanoparticles. The detected optical signals with M450 beads for 8.0, 2.0, 0.50, 0.125, 0.031, 0.007 HAU and NC were 2198 ± 233, 1199 ± 155, 774 ± 52, 531 ± 37, 462 ± 29, 390 ± 22, and 368 ± 15 mV (n = 3), respectively. By using the magnetic nanoparticles, the optical signals were approximately two times stronger than those from the M450 magnetic beads. This indicates that the proposed new system can successfully detect the influenza infection with a higher sensitivity. Furthermore, two negative samples (specimens 1 and 2) and three positive samples (specimens 3, 4 and 5) were applied for pre-clinical test in order to verify the developed microfluidic system. The optical signal for pre-clinical test of specimens 1, 2, 3, 4 and 5 were measured to be 1225 ± 191, 1140 ± 212, 2295 ± 120, 2500 and 1964 ± 258 mV (n = 3), respectively. The pre-clinical testing fluorescence images with nanoparticles were shown in Figure 6, *I* and the error bars of the signal from the nanoparticles were shown in Figure 6, *J*. These results show that the developed microfluidic system can distinguish the difference between the negative specimens and positive clinical specimens and further statistical analysis was shown in SI section IX.

Discussion

In this study, the nanoparticle production process was firstly applied to a nanosized-tunable $MnFe_2O_4$ nanoparticles synthesis. This process consisted of the size-control $Fe_{3-\delta}O_4$ and the shape-phase-control M–Fe–O nanoparticles production methods.[36,37] However, only approximately 20-nm nanoparticles were produced in the previous studies, thus increasing the required rounds of thermal decomposition of the $MnFe_2O_4$ nanoparticles to grow to approximately 100 nm. By using different synthesis temperatures (150, 270, and 305 °C), the manual operation steps were relatively safer and the shape and size of nanoparticles could be further controlled effectively. While these 100-nm nanoparticles were detected under the UV–Vis spectrum, the UV absorbance

range showed specific features of approximately 300 ~ 350 nm, which enables perceiving the color of the $MnFe_2O_4$ nanoparticles involved. Note that they were different from the $MnFe_2O_4$ nanoparticles obtained by using another production process, which showed a green color.[40]

XDR peaks showed the crystal phase pattern of the $MnFe_2O_4$. Compared with the standard $MnFe_2O_4$ pattern of JCPDS (10-0319), non-typical peaks were detected at 331, 531, and 444.[41] However, further comparisons with JCPDS patterns of 73-1964, 74-2403, 75-0034, and 88-1965 showed other XRD patterns of $MnFe_2O_4$ with slight differences in the formation ratios of Mn and Fe.[42–45] Future studies on nanocrystal formation and nanoparticle structures could benefit from using the $MnFe_2O_4$ nanoparticle synthesis method proposed in this study.

Another unique feature of this study involved successfully applying the appropriate PDMS surface modification methods for the $MnFe_2O_4$ nanoparticles. The final nanoparticles hydrophilic process caused them to carry a positive charge, thereby showing non-specific adhesion in the micromixer chamber. It even caused a high background signal of approximately 708 mV, as shown in Supplemental Figure 2. Subsequently, P123, PAA, and PEI were applied, and the PDMS surface modification method also produced a positive charge in the micromixer chamber. By applying this LBL self-assembly structure, these nanoparticles can mix well in the micromixer and lower the background noise to 440 mV. The findings of this research provide a new approach for nanoparticle application of dynamic mixing in a microfluidic system. Many types of surface modification methods should be adapted for different nanoparticles from different synthesis processes. Other PDMS surface modification methods should also demonstrate their function after further testing and produce stronger dynamic nanoparticle mixing signals and lower background noise.[46,47]

On average, the nanoparticles signal was twice stronger than that of the M450 micro-beads. To compare the signals between the M450 beads and the $MnFe_2O_4$ nanoparticles, the similar weight of beads/nanoparticles (approximately 6.1 μg per reaction) coated with α-A-NP mAbs (5 μg, as shown in section 2.4) were used. The difference in diameter between the two types of particles (4.5 μm for M450 beads versus 100 nm for nanoparticles) results in a difference of 2025 times in their surface areas. However, the number of applied M450 beads was totally 8.0×10^4, which was much less than the number of $MnFe_2O_4$ nanoparticles of the same weight (totally 2.2×10^9). These predicted results indicate that the nanoparticles contain approximately 10 times the reaction surface area of the M450 beads ($1 \times 2.2 \times 10^9$: $2025 \times 8.0 \times 10^4 \approx 10{:}1$). Therefore, there are two aspects of this research requiring further discussion. First, the collection of magnetic nanoparticles should be performed by comparing it with previous work on M450 beads.[19,20] Although the fluorescence signals were located in the nanoparticles, as the merged images shown in Figures 6, *A-G*, the nanoparticles may not be completely focused for better signals. Second, the error bar of the signal from the nanoparticles shown in Figure 6, *H* is higher than M450, and the background noise of 1× PBS control is also higher than the error bar of M450. Effective focusing and collection are the next concerns for applying dynamically mixed nanoparticles and combining dielectrophoresis; otherwise the AC electro-osmosis force may provide the additional force for nanoparticle collection.[48,49] In addition, a well-designed customer-made control system, which was composed of a temperature control module, an air compressor, several EMVs, and an optical detection module, might also reduce optical signal loss and automatically perform the entire diagnostic process.[50] Note that in this study only the limited number of clinical samples was applied and a much greater number of samples should need to be tested to fully validates this system for medical diagnosis in the near future.

This study is the first attempt to demonstrate an integrated microfluidic system that involves using dynamically mixed magnetic $MnFe_2O_4$ nanoparticles to detect the influenza infection with FIA. By using this approach and combining with LBL surface modification, the LOD of the on-chip diagnoses was improved to be as low as 0.007 HAU. The employment of the nanoparticles increased the FIA signal by approximately two-fold when compared with commercial 4.5-μm magnetic beads because of the large surface-to-volume ratio of the nanoparticles. This microfluidic system can automatically perform an immunoassay to detect the influenza infections within 20 min, thus showing promise for rapidly diagnosing infectious diseases.

Acknowledgments

The authors thank Dr. Sung-Yi Yang, Dr. Fong-Yu Cheng, and Mr. Po-Kai Chen for related experimental assistance and valuable discussions.

Appendix A. Supplementary data

Supplementary data to this article can be found online at http://dx.doi.org/10.1016/j.nano.2013.11.009.

References

1. Corbett EL, Watt CJ, Walker N, Maher D, Williams BG, Raviglione MC, et al. The growing burden of tuberculosis global trends and interactions with the HIV epidemic. *Arch Intern Med* 2003;**163**:1009-21.
2. Guan Y, Zheng BJ, He YQ, Liu XL, Zhuang ZX, Cheung CL, et al. Isolation and characterization of viruses related to the SARS coronavirus from animals in Southern China. *Science* 2003;**302**:276-8.
3. Hutson AM, Atmar RL, Estes MK. Norovirus disease: changing epidemiology and host susceptibility factors. *Trends Microbiol* 2004;**12**:279-87.
4. Horimoto T, Kawaoka Y. Influenza: lessons from past pandemics, warnings from current incidents. *Nat Rev Microbiol* 2005;**3**:591-600.
5. Chowell G, Bertozzi SM, Colchero MA, Lopez-Gatell H, Alpuche-Aranda C, Hernandez M, et al. Severe respiratory disease concurrent with the circulation of H1N1 influenza. *N Engl J Med* 2009;**361**:674-9.
6. Sala G, Cordioli P, Moreno-Martin A, Tollis M, Brocchi E, Piccirillo A, et al. ELISA test for the detection of influenza H7 antibodies in avian sera. *Avian Dis* 2003;**47**:1057-9.
7. Shibata T, Tanaka T, Shimizu K, Hayakawa S, Kuroda K. Immunofluorescence imaging of the influenza virus M1 protein is dependent on the fixation method. *J Virol Methods* 2009;**156**:162-5.
8. Boivin G, Côté S, Déry P, De Serres G, Bergeron MG. Multiplex real-time PCR assay for detection of influenza and human respiratory syncytial viruses. *J Clin Microbiol* 2004;**42**:45-51.

9. Gupta A, Akin D, Bashir R. Single virus particle mass detection using microresonators with nanoscale thickness. *Appl Phys Lett* 2004;**84**: 1976-8.
10. Ilic B, Yang Y, Craighead HG. Virus detection using nanoelectromechanical devices. *Appl Phys Lett* 2004;**85**:2604-6.
11. Choi JW, Ahn CH, Bhansali S, Henderson HT. A new magnetic bead-based filterless bio-separator for integrated bio-molecule detection systems. *Sensors Actuators B* 2000;**68**:34-9.
12. Zborowski M, Sun L, Moore LR, Williams PS, Chalmers JJ. Continuous cell separation using novel magnetic quadrupole flow sorter. *J Magnetism Magnetic Materials* 1999;**194**:224-30.
13. Gupta AK, Nair PR, Akin D, Ladisch MR, Broyles S, Alam MA, et al. Anomalous resonance in a nanomechanical biosensor. *Proc Natl Acad Sci U S A* 2006;**103**:13362-7.
14. Choi JW, Oh KW, Han A, Wijayawardhana CA, Lannes C, Bhansali S, et al. Development and characterization of microfluidic devices and systems for magnetic bead-based biochemical detection. *Biomed Microdevices* 2001;**3**:191-200.
15. Easley CJ, Karlinsey JM, Bienvenue JM, Legendre LA, Roper MG, Feldman SH, et al. A fully integrated microfluidic genetic analysis system with sample-in–answer-out capability. *Proc Natl Acad Sci U S A* 2006;**103**:19272-7.
16. Whitesides GM. Overview: the origins and the future of microfluidics. *Nature* 2006;**442**:368-73.
17. Lien KY, Lee WC, Lei HY, Lee GB. Integrated reverse transcription polymerase chain reaction systems for virus detection. *Biosens Bioelectron* 2007;**22**:1739-48.
18. Yang SY, Lien KY, Huang KJ, Lei HY, Lee GB. Micro flow cytometry utilizing magnetic bead-based immunoassay for rapid virus detection. *Biosens Bioelectron* 2008;**24**:855-62.
19. Lien KY, Hung LY, Huang TB, Tsai YC, Lei HY, Lee GB. Rapid detection of influenza A virus infection utilizing the immunomagnetic bead-based microfluidic system. *Biosens Bioelectron* 2011;**26**:3900-7.
20. Hung LY, Huang TB, Tsai YC, Yeh CS, Lei HY, Lee GB. A microfluidic immunomagnetic bead-based system for the rapid detection of influenza infections: from purified virus particles to clinical specimens. *Biomed Microdevices* 2013;**15**:539-51.
21. Patolsky F, Zheng G, Hayden O, Lakadamyali M, Zhuang X, Lieber CM. Electrical detection of single viruses. *Proc Natl Acad Sci U S A* 2004;**101**:14017-22.
22. Tegos GP, Demidova TN, Arcila-Lopez D, Lee H, Wharton T, Gali H, et al. Cationic fullerenes are effective and selective antimicrobial photosensitizers. *Chem Biol* 2005;**12**:1127-35.
23. Lu AH, Salabas EL, Schüth F. Magnetic nanoparticles: synthesis, protection, functionalization, and application. *Angew Chem Int Ed Engl* 2007;**46**:1222-44.
24. Lai W, Tang D, Que X, Zhang J, Fu L, Chen G. Enzyme-catalyzed silver deposition on irregular-shaped gold nanoparticles for electrochemical immunoassay of alpha-fetoprotein. *Anal Chim Acta* 2012;**755**:62-8.
25. Lum J, Wang R, Lassiter K, Srinivasan B, Abi-Ghanem D, Berghman L, et al. Rapid detection of avian influenza H5N1 virus using impedance measurement of immuno-reaction coupled with RBC amplification. *Biosens Bioelectron* 2012;**38**:67-73.
26. Massoud TF, Gambhir SS. Molecular imaging in living subjects: seeing fundamental biological processes in a new light. *Genes Dev* 2003;**17**: 545-80.
27. Weissleder R. Molecular imaging in cancer. *Science* 2006;**312**:1168-71.
28. Lee JH, Huh YM, Jun YW, Seo JW, Jang JT, Song HT, et al. Artificially engineered magnetic nanoparticles for ultra-sensitive molecular imaging. *Nat Med* 2007;**13**:95-9.
29. Kim KS, Park JK. Magnetic force-based multiplexed immunoassay using superparamagnetic nanoparticles in microfluidic channel. *Lab Chip* 2005;**5**:657-64.
30. Lin FYH, Sabri M, Alirezaie J, Li D, Sherman PM. Development of a nanoparticle-labeled microfluidic immunoassay for detection of pathogenic microorganisms. *Clin Diagn Lab Immunol* 2005;**12**:418-25.
31. Chen GD, Alberts CJ, Rodriguez W, Toner M. Concentration and purification of human immunodeficiency virus type 1 virions by microfluidic separation of superparamagnetic nanoparticles. *Anal Chem* 2010;**82**:723-8.
32. Teste B, Malloggi F, Siaugue JM, Varenne A, Kanoufi F, Descroix SD. Microchip integrating magnetic nanoparticles for allergy diagnosis. *Lab Chip* 2011;**11**:4207-13.
33. Shao L, Ren Z, Zhang G, Chen L. Facile synthesis, characterization of a $MnFe_2O_4$/activated carbon magnetic composite and its effectiveness in tetracycline removal. *Mater Chem Phys* 2012;**135**:16-24.
34. Beveridge JS, Stephens JR, Williams ME. The use of magnetic nanoparticles in analytical chemistry. *Annu Rev Anal Chem* 2011;**4**:251-73.
35. Weng CH, Huang TB, Huang CC, Yeh CS, Lei HY, Lee GB. A suction-type microfluidic immunosensing chip for rapid detection of the dengue virus. *Biomed Microdevices* 2011;**13**:585-95.
36. Kwok DY, Neumann AW. Contact angle measurement and contact angle interpretation. *Adv Colloid Interface Sci* 1999;**81**:167-249.
37. Huang CC, Chang CN, Yeh CS. A thermolysis approach to simultaneously achieve crystal phase- and shape-control of ternary M–Fe–O metal oxide nanoparticles. *Nanoscale* 2011;**3**:4254-60.
38. Huang CC, Chuang KY, Chou CP, Wu MT, Sheu HS, Shieh DB, et al. Size-control synthesis of structure deficient truncated octahedral $Fe_{3-\delta}O_4$ nanoparticles: high magnetization magnetites as effective hepatic contrast agents. *J Mater Chem* 2011;**21**:7472-9.
39. Sugiura A, Tobita K, Kilbourne ED. Isolation and preliminary characterization of temperature-sensitive mutants of influenza virus. *J Virol* 1972;**10**:639-47.
40. Liao MY, Huang CC, Chang MC, Lin SF, Liu TY, Su CH, et al. Synthesis of magnetic hollow nanotubes based on the Kirkendall effect for MR contrast agent and colorimetric hydrogen peroxide sensor. *J Mater Chem* 2011;**21**:7974-81.
41. Berbenni V, Marini A, Profumo A, Cucca L. The effect of high energy milling on the solid state synthesis of $MnFe_2O_4$ from mixtures of MnO–Fe_2O_3 and Mn_3O_4–Fe_2O_3. *Z Naturforsch* 2003;**58b**:415-22.
42. Hu P, Yu L, Zuo A, Guo C, Yuan F. Fabrication of monodisperse magnetite hollow spheres. *J Phys Chem C* 2009;**113**:900-6.
43. Sam S, Nesaraj AS. Preparation of $MnFe_2O_4$ nanoceramic particles by soft chemical routes. *Int J Appl Sci Eng* 2011;**9**:223-39.
44. Deraz NM, AlarifiInt A. Controlled synthesis, physicochemical and magnetic properties of nano-crystalline Mn ferrite system. *J Electrochem Sci* 2012;**7**:5534-43.
45. Huang CJ, Lin HI, Shiesh SC, Lee GB. Integrated microfluidic system for rapid screening of CRP aptamers utilizing systematic evolution of ligands by exponential enrichment (SELEX). *Biosens Bioelectron* 2010;**25**:1761-6.
46. Wong I, Ho CM. Surface molecular property modifications for poly (dimethylsiloxane) (PDMS) based microfluidic devices. *Microfluid Nanofluidics* 2009;**7**:291-306.
47. Zhou J, Khodakov DA, Ellis AV, Voelcker NH. Surface modification for PDMS-based microfluidic devices. *Electrophoresis* 2012;**33**:89-104.
48. Kadaksham AT, Singh P, Aubry N. Dielectrophoresis of nanoparticles. *Electrophoresis* 2004;**25**:3625-32.
49. Chiou PY, Ohta AT, Jamshidi A, Hsu HY, Wu MC. Light-actuated AC electroosmosis for nanoparticle manipulation. *J Microelectromech S* 2008;**17**:525-31.
50. Chang WH, Yang SY, Wang CH, Tsai MA, Wang PC, Chen TY, et al. Rapid isolation and detection of aquaculture pathogens in an integrated microfluidic system using loop-mediated isothermal amplification. *Sens Actuators B Chem*. http://dx.doi.org/10.1016/j.snb.2011.12.054